ISME

Numerical Study of the Tongue Geometry Effects on the Cavitation and Performance of a Centrifugal Pump in Off-design Conditions

M. Mahdi*
Assistant Professor

S. V. Sajadi†
M.Sc.

M. Rasekh‡
M.Sc.

In this study, the effects of the volute tongue geometry variation on the head, efficiency, velocity distribution and cavitation structure of a centrifugal pump in the steady flow behavior under off-design conditions have been investigated. Numerical simulation modeling based on the $k-\omega$ turbulence model with a hybrid grid is used to simulate the flow within the modeled pump. The flow is simulated by means of a commercial Computational Fluid Dynamics (CFD) software that solved the Reynolds-averaged Navier-Stokes (RANS) equations for a three-dimensional steady flow. The effects of thickness and angle of the tongue in various flow rates on the pump performance is investigated. Numerical results which are in well agreement with the experimental ones, show that the higher tongue angles caused an improvement on the head and efficiency of the pump especially in high flow rates. Investigations also indicate that the tongue thickness variations have no significant impact on the pump performance, although, the lower the thickness, the better the overall pump performance.

Keywords: centrifugal pump, cavitation, off-design conditions, volute tongue, computational fluid dynamics, two-phase flow

1 Introduction

One of the most common devices used in industries are pumps. Pumps are mechanical devices employed to transfer fluids from one point to another, or from a pressure or energy level to another pressure or level [1]. Centrifugal pumps are more important than other pumps because of their simple constructional form, low volume to power consumption ratio and abundant variety of utilization items. Flow field within centrifugal pumps is a strong three-dimensional flow with rotational input and output flows, flow separation, cavitation, etc [2].
Geometry of the impeller is also complex rotating to the volute casing. Strong interaction between the impeller and the volute tongue is responsible for the instability of flow field within the volute casing [3].

* Corresponding Author, Assistant Professor, Department of Mechanical Engineering, Shahid Rajaee Teacher Training university, m.mahdi@sru.ac.ir
† M.Sc., Department of Mechanical Engineering, Shahid Rajaee Teacher Training university, sajjadi.vahid@yahoo.com
‡ M.Sc., Department of Mechanical Engineering, Shahid Rajaee Teacher Training university, saeedrasekh3@gmail.com
Receive : 2019/05/20 Accepted : 2019/07/14

Also, flow structures diverted from the impeller to the volute casing can have further growth because of the rotational flow, resulting in more kinetic energy losses. Among the various pump geometrical parameters, such as inlet, impeller, volute casing (circular wall), tongue shape in casing and cross-sectional area of throttle, volute casing and tongue play a major role in performance control in off-design conditions [4]. This important role shows that a correct choice of the tongue area (for instance, the angular position of the tongue) is necessary for the best design of the volute casing. Once a centrifugal pump is working at low flow coefficients, for example, near or below 50% of design conditions, the flow gets close to the impeller blades with relatively high angles of incidence. As a result of strong interactions due to the development between the flow and impeller blades, a recirculation specified by the considerable axial and azimuthal components of the flow vorticity is formed at the low-pressure area near the impeller eye. At low enough cavitation parameters, the centrifugal pressure gradients in these vortical areas will be able to grow the cavitation rapidly due to the backflow and development across considerable distances of the impeller eye upstream. Meanwhile, cavitation is also developing in the impeller blades suction side, where the pressure drop values are decreased sufficiently [5]. Besides, at the tip of the blades, flow leakage cavities, exposing to low pressure gradients, are pulled to the backflow. The growth and collapse duration of the cavities thereupon increase that let them be shifted across relatively large distances of the upstream flow of the impeller [6]. It should be noted that this process is unstable and an alternate sloshing oscillating motion which can maintain a stable auto-oscillation that is typically developed in the frequencies lower than the rotational pump shaft frequency is occurred [7]. The instability of this low flow rate is able to cause intense vibrations in the pump inlet line, and also intense oscillations in forces of the impeller, causing tensions often lead to failure of the pivotal bearings, and even sometimes to the pump shaft incision [7]. Many experimental and numerical studies have been conducted for investigating the centrifugal pump flow, and each of them has examined a part of the pump. In this case, Hira & Vasandani [8], examined the radial clearance effects between the outlet of the impeller and the volute tongue by changing the volute tongue length or the tongue starting angle. Their laboratory results show that the maximum efficiency point is shifted to lower flow rates by increasing the radial clearance, or reducing the tongue length or the tongue angle. Gonzalez et al. [9] have studied the radial gap variation effects of a centrifugal pump on its impeller numerically and verified it by means of experimental investigations. They approved that the pressure oscillations on any place of the volute are basically not established by the effects of the radial gap change from 15.8% to 10% of the impeller radius. Wong et al. [10] have examined the effects of the tongue position and the base circle diameter on the performance of a centrifugal blood pump. The average velocity method has been used to determine the volute profile. Based on their simulations, a tongue position of 15 degrees was recommended because the pressure head was almost comparable to the maximum head developed with a reduced net radial force. According to Guo et al. [11], numerical simulations on impeller-volute interactions in a centrifugal pump with low specific velocity investigating the effects of change in outlet diameter of the impeller and tongue profile variation on the flow field using a commercial code CFX-10 was studied. Results show that the effect of various profiles on stability of a centrifugal pump is considerable and significant. The high-efficiency range of a centrifugal pump can be extended to some limited values, in other words, when a sharp tongue is substituted for a middle one, the maximum efficiency point is shifted toward the higher flow rates. Raul Barrio et al. [12] provides a numerical study on the pulsating flow in the tongue area for a conventional centrifugal pump with an impeller-tongue gap that is 11.4% of the impeller radius. Numerical simulation of the unsteady flow (3D-URANS + $k-\varepsilon$ model) was done by a Fluent commercial code. After validating, the numerical model was also used to evaluate the evolution of the leakage flow between the impeller-tongue gap and of the flow exiting the impeller with some angular intervals.

Bachert et al [13] studied an isolated flow in a centrifugal pump working in overload conditions where cavitation in the tongue of the volute casing is occurred more than in the impeller. In this case, the standard threshold of 3% head loss is not caused by this type of cavitation in the impeller, but is due to the cavitation on the volute tongue. Fu et al. [6] studied the features of flow instabilities and cavitation in a centrifugal pump in low flow rate conditions using the numerical and experimental tools, respectively. In general, heat and mass transmission between liquid and vapor phases, in addition to the surface tension effects, are simultaneously associated with the cavitation. Their experimental results showed that the unsteady behavior of the internal flow in the centrifugal pump operating at low flow rates has the characteristics of a peculiar low-frequency oscillation. In addition to that, the hydraulic performances of the centrifugal pump, predicted by numerical simulations, were in good agreement with their experimental data. Alemi et al. [14] investigated the effects of the volute tongue geometry variation on the head, efficiency and radial force of a centrifugal pump using numerical simulation modeling based on $k-\omega$ turbulence model, applied in CFX-13. Their results revealed that a large cutwater gap, a short tongue volute and also a tongue angle of 5° less than the impeller outlet velocity angle, caused lower radial force. Gu et al. [15] simulated the transient turbulent flow in the whole flow field of a low-specific-speed centrifugal pump by employing the Reynolds-averaged Navier-Stokes equation coupled with $SST-k-\omega$ turbulence model, and their numerical results agree well with the experimental curves. It was deduced from their study that splitter blades produce more unsteadiness and energy dissipation than main blades. Jia et al. [16] simulated a prototype centrifugal pump at different flow rates and verified them to available experimental data. The numerical results which was gathered from Fluent software using 3D URANS equations, showed that with increasing of flow rate, the proportion of local high-pressure region in impeller passage decreases and the flow becomes smoother accordingly. Yan et al. [17] studied on a double suction centrifugal pump and investigated the influences of the tongue shape on the flow characteristics at the near-tongue region. Their numerical simulation showed that under small flow conditions, the head and efficiency of the short-tongue model are higher than that of the middle-tongue and longue-tongue models.

Also, under large flow conditions, the head and efficiency curves of the three models are relatively close. Recently, Oro et al. [18] analyzed the deterministic stresses caused by the interactions between the impeller and tongue of a single volute centrifugal pump. Their numerical 3D model was developed using ANSYS-Fluent benefiting from the RNG $k-\varepsilon$ turbulence model in URANS equations. They concluded that turbulent structures are important only in off-design conditions and also persist in the vicinity of the volute tongue. Besides, they showed that the tongue has a significant impact on the impeller flow structures, but the impeller wakes have no effect over the flow structures of the volute tongue. Furthermore, Arani et al. [19] investigated the tongue effects on the performance and radial force of a centrifugal pump in a low specific speed, numerically. Their CFD results, obtained by the $k-\omega$ turbulence model, indicated that the tongue geometry affect the radial force and performance of the specified centrifugal pump in both direct and reverse mode, significantly. Also, they found that the tongue with the most stretching has the lowest head value in high flowrates and is exposed to an efficiency reduction. Many efforts have been made recently by various scientists to improve the overall pump performance and among the different strategies, volute tongue variation have gained very much attention. Until now, there is not any specific study aimed to investigate the effects of tongue geometry, including angle and thickness, on the hydraulic performance, head loss, pump efficiency and, velocity contour and vapor structure in the vicinity of the tongue in off-design conditions. In this research, using CFD techniques, first the simulation is carried out on the pump model with available laboratory results in the study of Fu et al. [6] and then, appropriate turbulence and cavitation models have been selected.

Next, in the steady state with a change in geometric shape of the tongue, including the leading edge thickness and the angular position of the tongue, in various boundary conditions, the simulation is conducted. Afterwards, the cavitation outside of the design conditions at the tongue area of the centrifugal pump is investigated.

2 Governing equations

For modeling a flow with cavitation, the type of the turbulence model, type of the flow, and boundary conditions should be selected proportional to the flow to obtain a proper numerical method to achieve favorable results. In this research, the method chosen for the two-phase flow is the homogeneous mixture and the governing equations (continuity and momentum) are provided proportion to that. The modeling of the cavitation flow in the centrifugal pump model which was done by ANSYS Fluent V16 make use of quasi-homogeneous multi-phase cavitation modeling. In this model, it is supposed that two phases have the same velocity and temperature but different pressures, which are used in association with Rayleigh–Plesset Equation (RPE) to assess the local intensity of the vapor or condensate production. There are similar RPE models that have been based widely for the numerical cavitation analysis without any limitations between flow fields with higher and lower flow rates such as Zwart-Gerber-Belamri (ZGB) model [20] which is also available in FLUENT software and can be used by assuming the constant evaporation pressure, diameter of bubble, mass ratio of core position, vaporization and condensation coefficients (F_{vap}, F_{cond}) as inputs. Investigating the researches shows that the results of $k-\varepsilon$ turbulence model have closer values to the laboratory ones. So, this model has been chosen to be used in the analyses. Governing equations of two-phase flow based on the homogeneous mixture approach, considering the mixture as a fluid under a homogeneous mixture model, is investigated. The flow field will be solved using equations of continuity and momentum which are formulated respectively as below [21]:

$$\frac{\partial}{\partial t}(\rho_m) + \nabla.\left(\rho_m \vec{V}_m\right) = 0 \qquad (1)$$

$$\frac{\partial}{\partial t}\left(\rho_m \vec{V}_m\right) + \nabla.\left(\rho_m \vec{V}_m . \vec{V}_m\right) = -\nabla p + \nabla.\left[\mu_m(\nabla\vec{V}_m + \nabla\vec{V}_m^T)\right] + \rho_m \vec{g} \qquad (2)$$

In which $\vec{V}_m$ is the mixture velocity vector, and density and viscosity of the mixture are as follows, respectively:

$$\rho_m = r_l \rho_l + r_v \rho_v \qquad (3)$$

$$\mu_m = r_l \mu_l + r_v \mu_v \qquad (4)$$

where ρ_m, r_l, ρ_l, r_v and ρ_v in equation (3) are the mixture density, the liquid volume ratio, the liquid density, the vapor volume ratio and the vapor density, respectively. Furthermore, μ_m, μ_l and μ_v are, respectively, the viscosity of the mixture, the liquid and the vapor.

The mixture model allows the process of diffusion levels. In a control volume, r_v and r_l values can have a certain amount, considering the occupied space of liquid or vapor phase. The subscripts l and v are for pure vapor and liquid features, respectively which are constant. The vapor, considered in cavitation area, contains small spherical bubbles. If the bubble radius is considered to be R_B, then r_v value is calculated as follows:

$$r_v = \frac{v_v}{v_l + v_v} = \frac{n_o \dfrac{4\pi R_B^3}{3}}{1 + n_o \dfrac{4\pi R_B^3}{3}} \qquad (5)$$

Where n_o is defined as the number of bubbles per unit volume of pure liquid.

The RPE, derived from the balance of momentum in the absence of thermal effects, interpreting the growth of gas bubbles in a liquid, is determined as follows:

$$R_B \frac{d^2R_B}{dt^2} + \frac{3}{2}\left(\frac{dR_B}{dt}\right)^2 + \frac{2S}{\rho_l R_B} = \frac{P_{sat} - P}{\rho_l} \tag{6}$$

where P and S are, respectively, the static pressure, and the coefficient of surface tension between the liquid and vapor. Also, P_{sat} refers to the saturation pressure for vapor. By not considering the second-order terms as well as the surface tension, the equation is reduced to:

$$\frac{dR_B}{dt} = \sqrt{\frac{2}{3}\frac{|P_{sat} - P|}{\rho_l}} \tag{7}$$

This equation considers the physical approach for studying the dynamic effects of a bubble in the cavitation model. By multi-phase modeling of the cavitation, the two-phase cavitation model could be used. This model includes the use of the standard viscous flow equations and a contractual turbulence model. It is noteworthy to mention that the specified viscous flow equations govern the mixture transmission (mixture model), or phases (multi-phase Euler model). In the cavitation, liquid-vapor mass transmission is performed using the vapor transmission equation, formulated as below:

$$\frac{\partial}{\partial t}(r_v\rho_v) + \nabla.(r_v\rho_v V_v) = R_e - R_c \tag{8}$$

where V_v represents the vapor phase velocity. Besides, R_e and R_c denote the spring terms of mass transmission which are relatively depend on the growth and collapse of vapor bubbles, respectively.

Assuming that all the system bulbs have the same sizes, Zwart-Gerber-Belamri [20] suggested that all the in-phase mass transmission rate per unit volume, R, using the number of bubble density, n_o, is calculated using equation (7). Besides, net mass transmission is equal to:

$$R = n_o \times \left(4\pi R_B^2 \rho_v \frac{dR_B}{dt}\right) \tag{9}$$

Vapor volume fraction, r_v, depending on density of bubbles number, n_o, and radius of bubble, R_B, is as follows:

$$r_v = n_o \times \left(\frac{4}{3}\pi R_B^3\right) \tag{10}$$

By inserting n_o value of the equation (9) in equation (10), the mass transmission expression will be as follows:

$$R_e = \frac{3r_v\rho_v}{R_B}\sqrt{\frac{2}{3}\frac{|P_{sat} - P|}{\rho_l}} \tag{11}$$

In equation (11), the mass transmission rate per unit volume only depends on the vapor phase density (ρ_v).

Equation (11) is derived by assuming the bubble growth (evaporation). In order to use the equation for collapse process of the bubble (condensation), the following equation is used:

$$R_e = F\frac{3r_v\rho_v}{R_B}\sqrt{\frac{2}{3}\frac{|P_{sat} - P|}{\rho_l}}\, sign(P_{sat} - P) \tag{12}$$

F is the empirical calibration coefficient in the above equation.

The nucleation site volume fraction must decrease appropriately as the vapor volume fraction grows .To model this process Zwart-Gerber-Belamri suggested to replace r_v with $r_{nuc}(1 - r_v)$ in equation (12). At last, the ultimate forms of this cavitation model are given by the following equations [22]:
if $P \leq P_{sat}$,

$$R_e = F_{vap} \frac{3r_{nuc}(1 - r_v)\rho_v}{R_B} \sqrt{\frac{2}{3} \frac{|P_{sat} - P|}{\rho_l}} \tag{13}$$

and, if $P \geq P_{sat}$,

$$R_c = F_{cond} \frac{3r_v(1 - r_v)\rho_v}{R_B} \sqrt{\frac{2}{3} \frac{(P - P_{sat})}{\rho_l}} \tag{14}$$

In the above two equations, F_{vap} and F_{cond} take the values of 50 and 0.01, respectively; R_B is the radius of bubble and is assumed to be 10^{-6}m; r_{nuc} represents the nucleation site volume fraction and its default value is assumed to be 5×10^{-4}.

3 Validation

In order to examine the accuracy of simulation results, first a centrifugal pump model with available laboratory results is modeled and investigated. Figure (1) shows the model geometry with available laboratory results. The model contains a six-bladed stimulus, a volute, and proper parts of inlet and outlet ducts. The general and main sizes of the pump in this study are reported in Tables (1, 2).
For simplifying, in the simulations of the present centrifugal pump performance, the flow between sheathed impeller, and, front and back surfaces of the shell has been overlooked. Considering the available three-dimensional model of the pump, grid generation can be carried out. Figure (2) shows the three-dimensional model of the pump and its established grid. In order to prevent an increase in calculation volume, an unstructured grid has been used. Beside, for sufficiently small wall edge area, a boundary layer grid is used at the edge of wall.

Figure (3) shows the hybrid grid established in the flow field within the pump.

(A)

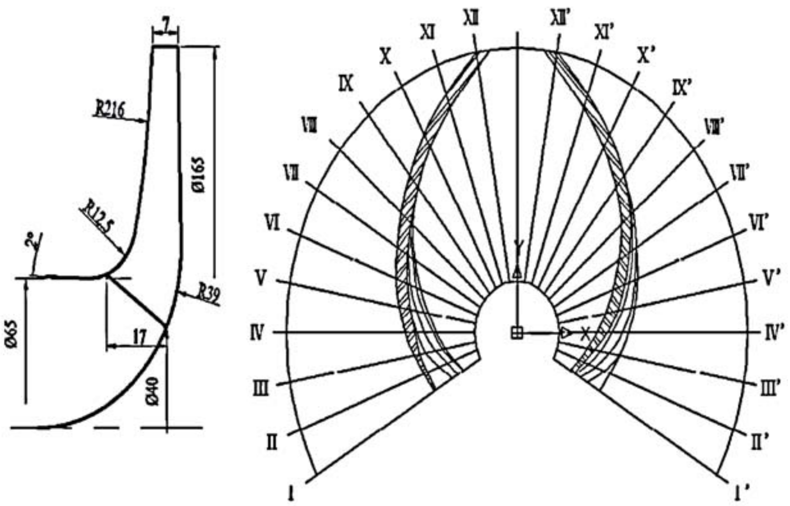

(B)

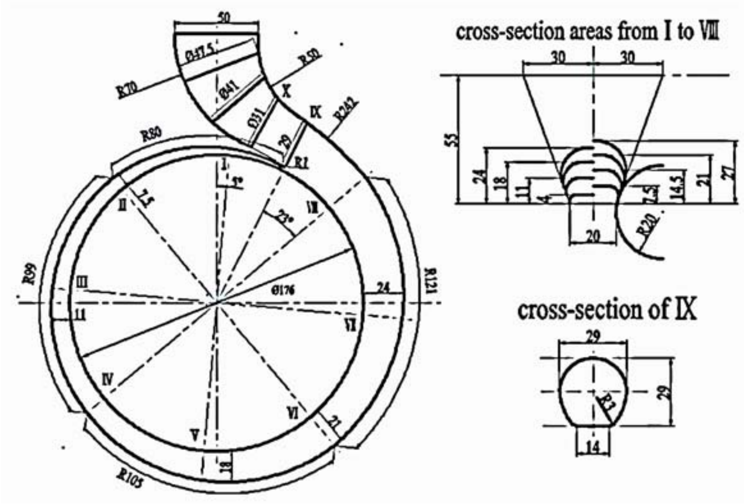

Figure 1 A two-dimensional view of A) impeller, B) Volute [6].

Table 1 Technical characteristics for design of the sample centrifugal pump [6]

Model	$Q_d(m^3/h)$	$H_d(m)$	$N(rpm)$	$NPSH_{3\%}(m)$	n_s
IS65-50-160	25	32	2900	1.6	66

Table 2 Geometric characteristics of the sample centrifugal pump [6]

Blade thickness at leading edge (mm)	α (deg)	β_1 (deg)	β_2 (deg)	b_3 (mm)	b_2 (mm)	d_h (mm)	Z $(No.)$	D_3 (mm)	D_2 (mm)	D_1 (mm)
0.7	14	28	30	20	7	40	6	176	165	65

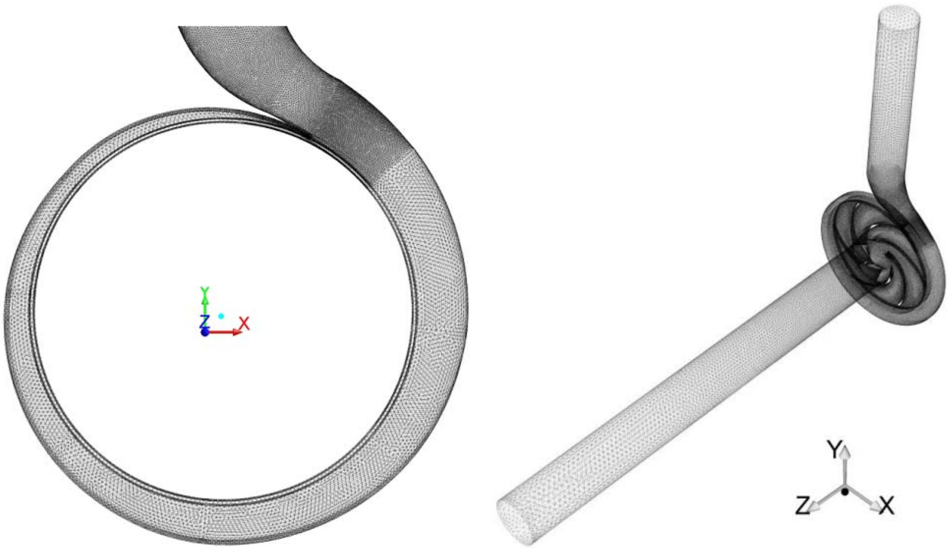

Figure 2 The centrifugal pump and its volute CFD model grid.

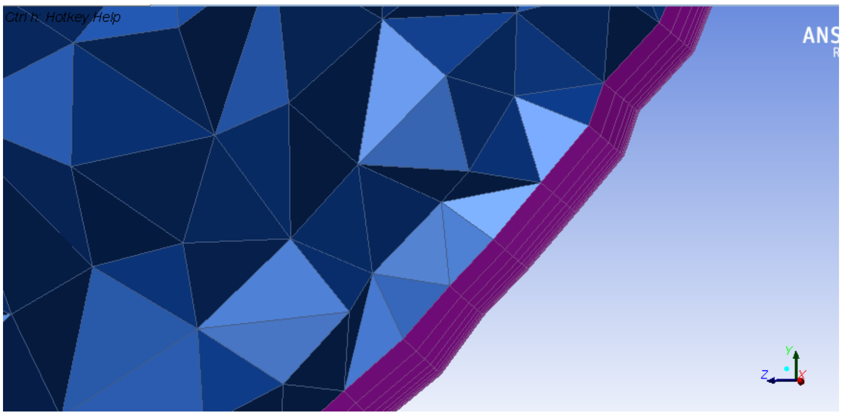

Figure 3 Boundary layer model and hybrid grid within the impeller.

Refining the mesh causes an improvement in the accuracy of simulations, however, the solution time and the required memory are also increased, while no unique solution is provided. In this case, the resolution of the mesh has been improved by focusing on the experimental results.

In particular, three types of computational grids (coarser, medium, and finer) are summarized in Table (3). Afterwards, as shown in Table (4), the pump head prediction remains approximately constant, when the medium and finer grids are used. The relative velocity distribution in the centrifugal pump in the design and loading conditions of a blade is particularly investigated based on various grids. Therefore, the similar medium grid has been used to provide simulation for significant saving of time and CPU cache with acceptable degree on the computational accuracy. y^+ values in any computational domain for inlet, impeller, volute, and outlet is, respectively, 1.4, 1.9, 1.1 and 0.87.

Table 3 Mesh size details

Computational domain	Inlet pipe	Impeller	Volute casing	Outlet pipe	Total
Number of mesh cells (coarser)	25482	190814	133733	6448	362468
Number of mesh cells (medium)	63840	271543	507240	24800	899105
Number of mesh cells (finer)	498735	1936784	2593709	226804	3454740

Table 4 Examining the independence of the centrifugal pump head grid in design conditions

Percentage of error %	Experimental head $H_{exp}(m)$	Numerical head $H_{nm}(m)$	Grid type
-2.26	34.98	35.77	Coarser grid
1.60	34.98	34.42	Medium grid
0.69	34.98	34.74	Finer grid

After modeling and mesh generation, the boundary conditions are defined as inlet pressure at the entrance of inlet and mass flow rate in the outlet boundary. For the working fluid, water is chosen at 25$^{\circ}C$ with saturation pressure of 3574 Pa. Also, the average diameter of the nucleation site is determined to be [23] 2×10^{-6}. The method used to determine the turbulence model in the inlet and outlet of the flow is the hydraulic diameter, and the turbulence intensity is considered to be 5%. The non-slip condition with roughness constant of 0.5 is determined for wall boundaries. An interface is chosen between the volute and the impeller meshes. The solution method is based on the control volume to convert the governing equations to the algebraic equations to be solved numerically. Besides, the segregated solver is used with absolute velocity formula, and SIMPLE algorithm is the pressure-velocity coupling scheme. For discretization of diffusive, convective and turbulent terms, the second order upwind is chosen in this research. Boundary conditions, the model of cavitation and the value of its parameters, and physical properties of the working fluid needed for the numerical simulation is shown in Table (5).

Experimental data were used to verification of the accuracy of the both $k-\omega$ and $k-\varepsilon$ turbulence models. Figures (4-a,b) show the total performance curves of the test pump in both experimental and CFD approaches. The overall performance prediction of the pump, done by numerical simulations, is in acceptable accordance with experimental and particularly the numerical data from Fu et al. [6] . Maximal difference between results of CFD simulation assuming $k-\omega$ and $k-\varepsilon$ turbulence models and experimental results are in the assumed range of flow rates about 8 % and 25% respectively. In this case $k-\omega$ model seems to be more suitable for CFD simulation of the flow in mixed - flow pump. The considering grid established based on the $k-\omega$ turbulence model is sufficiently dense at the edge of the wall which its y^{+} value equals to 1. Comparing the pump head shows that there is a slight difference between numerical and experimental results. Consequently, for numerical simulation of the pump flow, the $k-\omega$ turbulence model is used in the present study with acceptable error percentage.

All the simulations have been done using the following system specifications:

[Window 8, Intel(R)-Core(TM) i7 CPU E5507, x64 bit, 2.26 GHz, 32 GB RAM].

Table 5 Boundary conditions and physical properties for numerical simulation

	Thermodynamic parameters	Liquid phase	Vapor phase
Fluid physical properties	Density (kg/m^3)	998.2	0.5542
	Viscosity (kg/m-s)	0.001003	1.34×10^{-5}
	Specific heat (j/kg-k)	4182	2014
	Standard temperature (K)	298	298.15
	Vapor pressure (Pa)	3574	-
Flow boundary conditions	Input boundary condition	Total Pressure of inlet =101325 Pa	
	Outlet boundary condition	Mass-flow rate	
	Operating pressure (Pa)	0	
	Inlet and outlet turbulence intensity	Turbulence Intensity = 5 %	
	Input hydraulic diameter	Hydraulic Diameter = 65 mm	
	Output hydraulic diameter	Hydraulic Diameter = 50 mm	
Cavitation parameters	Cavitation model	Zwart-Gerber-Belamri(ZGB)	
	Bubble diameter (mm)	0.002	
	Volume fraction of the nucleation site	5×10^{-4}	
	Vaporization coefficient (F_{vap})	50	
	Condensation coefficient (F_{cond})	0.01	

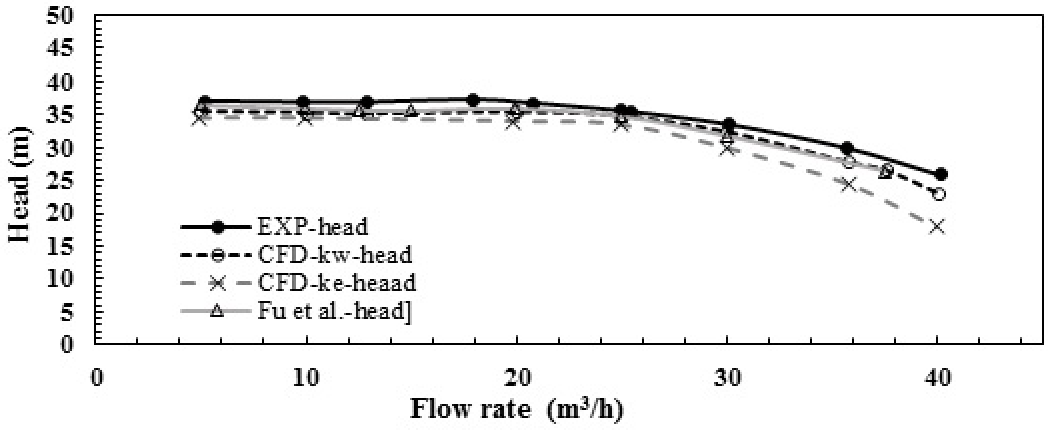

(a)

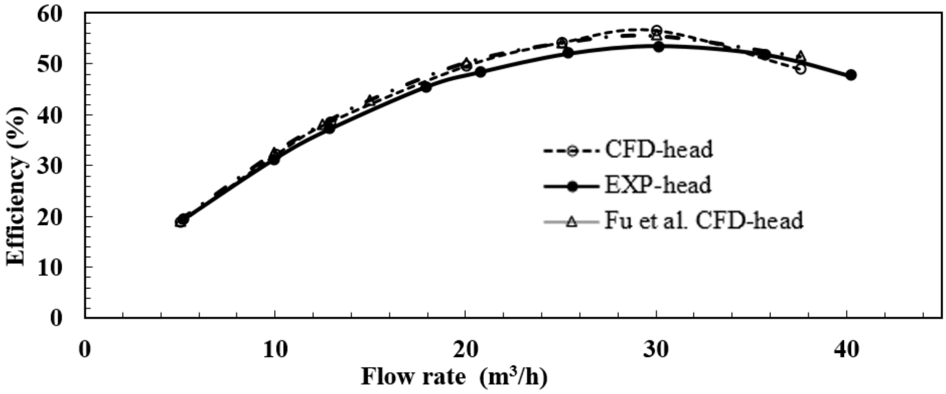

(b)

Figure 4 Hydraulic performance of the centrifugal pump in a) head and b) efficiency along flow rate.

The development of cavitation features in the pump model are simulated in low, design, and high flow rates, for example, in 40%, 100%, 120%, 150%, 160% of the design flow rate value, Q_a. The decline features of the head have been shown in Figure (5). In 100% and 120% of Q_a, as can be seen in Figure (5), the head loss curves show a sudden but regular head loss, as expected in the centrifugal pumps under cavitation conditions. In flow coefficients higher than 120%, the head loss features show a slight decrease of head in mid-levels of Net Positive Suction Head (NPSH) and actually in cavitation rate, right before the start of head curve decline. In addition to this slight head loss, a sudden head loss is also found but regularity is reduced.

In flow conditions lower than the design conditions 40% of Q_d, a cusp in the head performance curve is seen before the severe head loss, in addition that the NPSH is still decreased. The functional features in Figure (5), consistently along with experimental observation would approve that the start value of NPSH for the beginning of the cavitation effect on pump head is increased in low flow rates and as the flow rate is decreased, which is expected since the blade loading is increased.

The same features have been observed by Friedrichs & Kosyna [24; 25] and also by Hofmann et al. [26] in their experimental study on the head loss curves in centrifugal pumps with low certain velocity. In particular, they also observed a very similar behavior of head loss curve in relevant working points with cavitation and rotational oscillations related to the combined lift augmentation on the impeller blades which also could arise from the redistribution of the suction pressure due to the cavitation expansion. The additional curves of $NPSH_{3\%}$ and $NPSH_{10\%}$ as the parameters for the cavitation occurrence is shown and examined in Figure (6).

A special feature of this impeller based on the curve under cavitation conditions is that as the Q/Q_d coefficient value is reduced from 1.2 to 0.4, the NPSH$_{3\%}$ value is also decreased. According to the experimental observations, applying a large angle for the inlet blade of impeller, causing a high positive angle of collision in the design condition, could be the reason for the aforementioned problem. Another special feature of this impeller based on the curve under cavitation conditions is, as the Q/Q_d coefficient value is reduced from 1.6 to 1, a reduction in NPSH$_{3\%}$ and NPSH$_{10\%}$ is seen.

Steady cavitation simulations in low flow rates could be used for cavitation developments in the impeller differently depending on various flow rates. For this purpose, the volume distributions of attached cavitation on the impeller blades in the equivalent flow coefficients with 0.4 and 1.2 of design value are shown in Figures (7,8), respectively, where the six-blade channels have been numbered clockwise, contrary to the impeller rotation.

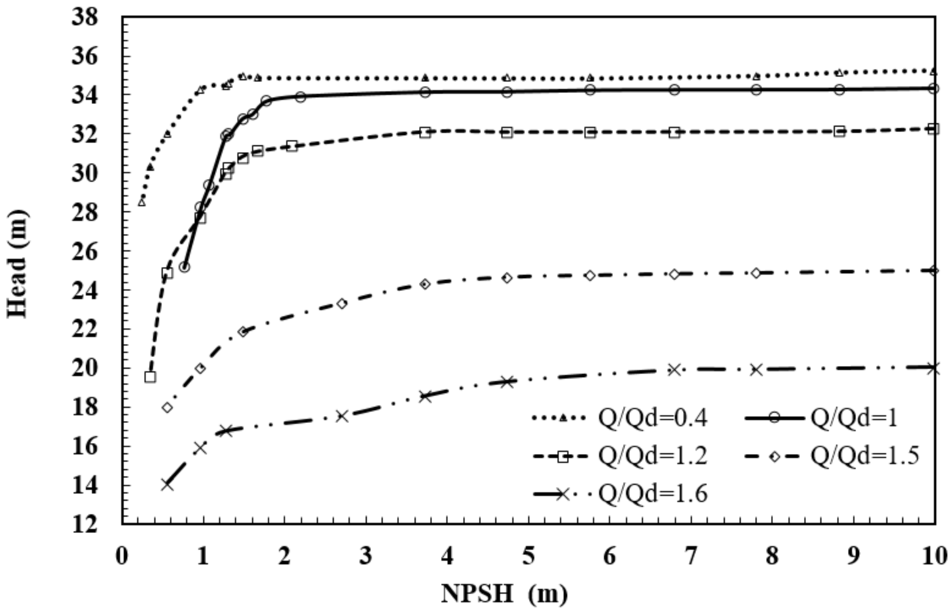

Figure 5 Head loss curves due to the centrifugal pump NPSH.

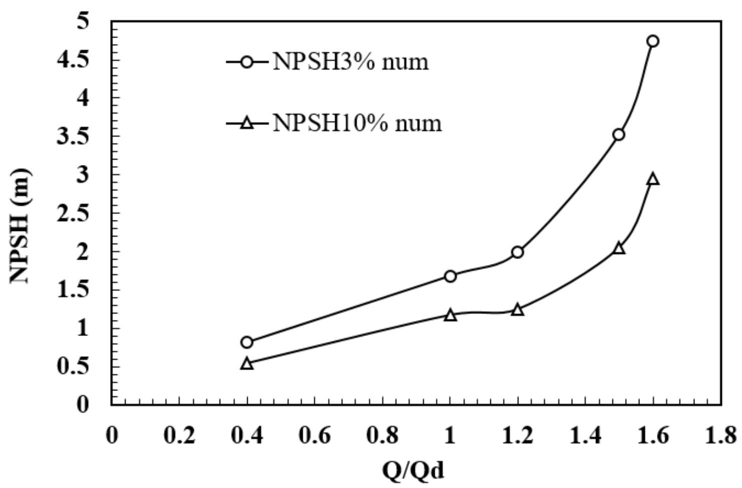

Figure 6 NPSH$_{3\%}$ and NPSH$_{10\%}$ curves of the centrifugal pump.

For the overall inlet pressures equal to 18000, 16500, 16000, and 13000 Pa, the cavities are relatively small and thin, and greatly developed on the suction side of the blade, as have been shown in the Figures (7 a-d). Furthermore, the thickness of cavities in the third blade channel is quite small. Further analyses show that the complete asymmetric cavitation vanishes in the higher flow rates, as shown in Figure (5). Particularly, Figures (8a,b) show that for a pump worked at 120% of the design flow rate, and 18000 and 16500 Pa of inlet pressures, respectively, small and thin cavities are attached uniformly toward the suction of blades, but as the inlet pressure is reduced, the vapor volume is almost increased uniformly on each blade, as shown in Figures (8c-f). The axisymmetric pressure distribution in the outlet of the impeller gets closer to the critical conditions leading to a further development of cavitation in channels of the blades, which is probably the reason that why no asymmetric cavitation occurred in these flow conditions.

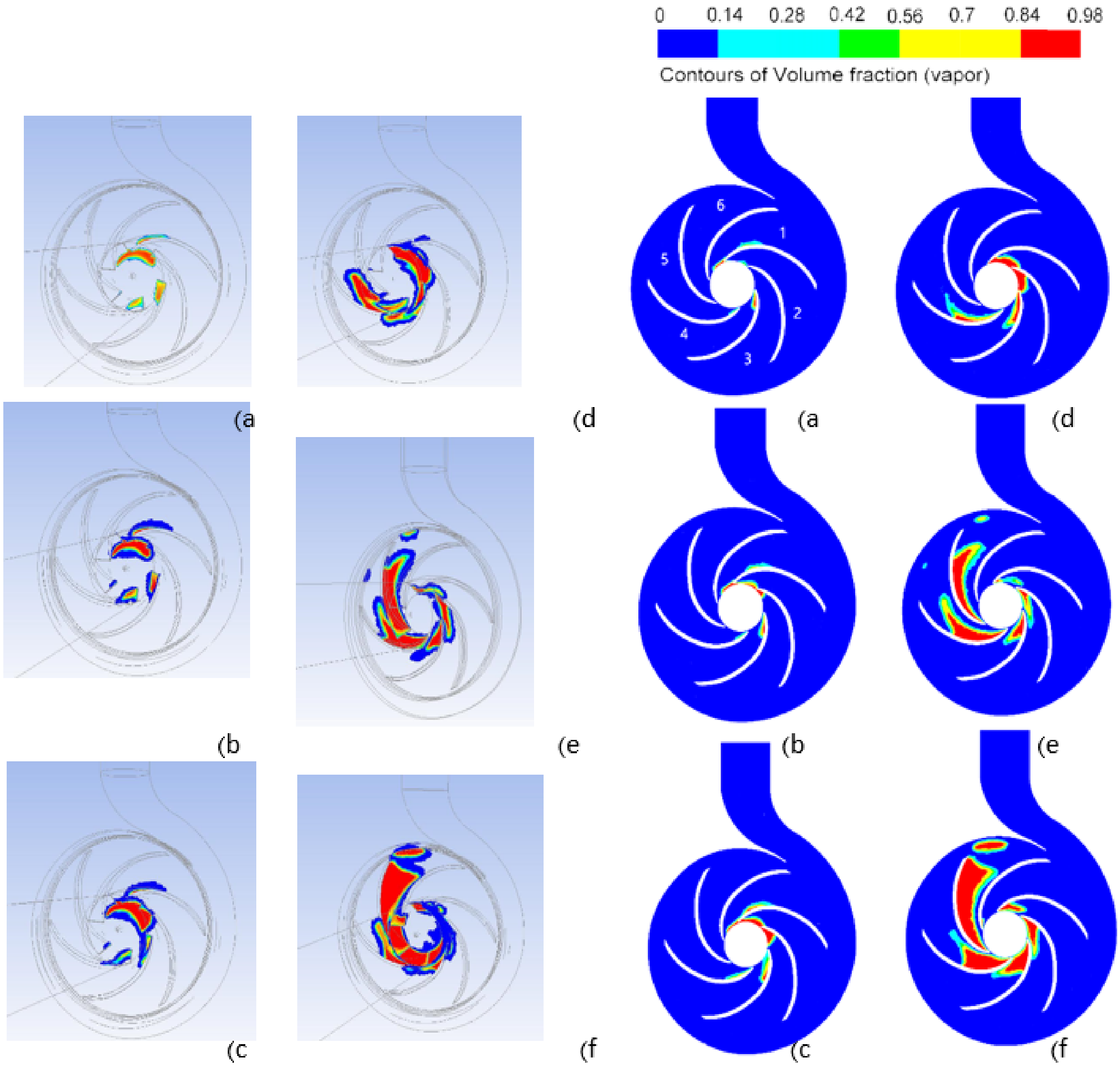

Figure 7 Vapor structures in cross sections of the modeled pump impeller at 0.4 of the Q_d for decreasing total pressures in the inlet.

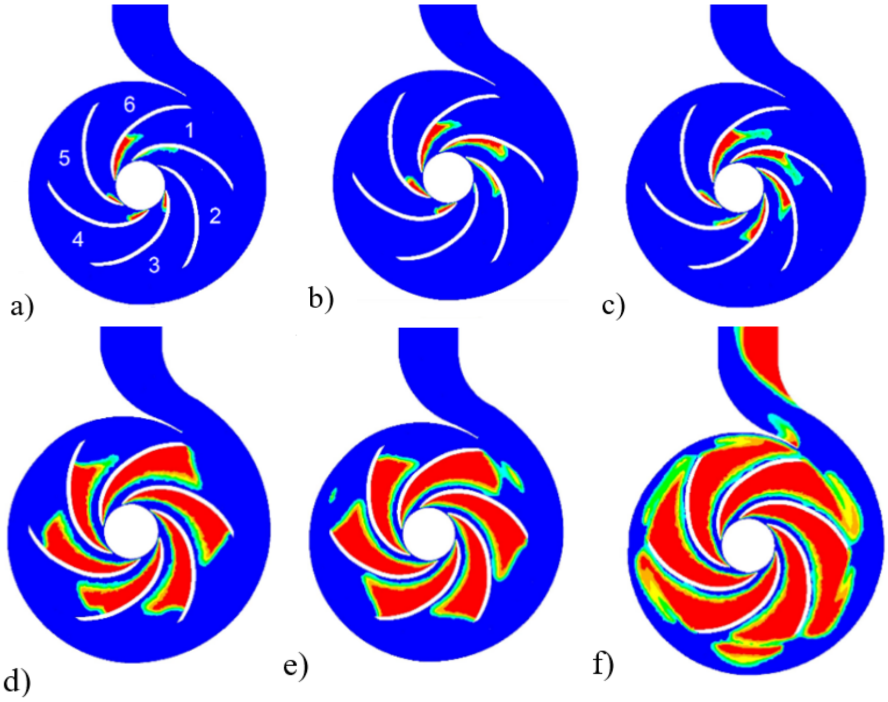

Figure 8 Vapor structures in cross sections of the modeled pump impeller at 1.2 of the Q_d for decreasing total pressures in the inlet.

4 Examining the effects of tongue profile variation on efficiency of the centrifugal pump

The starting point of the volute profile is the volute tongue and the circle passing through this point is called the base circle. The base circle diameter is specified by D_3. Usually, the base circle diameter is a little larger than the impeller outlet diameter D_2. The minimum gap between the impeller diameter and the volute base circle should be maintained to allow the flow to discharge slowly from the impeller to the volute. The minimum redial gap is a critical factor affects the volute flow conditions, especially, when the pump is working under off-design conditions. In flow rates lower than the design flow rate, the volute tongue deflects the amount of flow approaching the throttle, which causes a bulk flow to re-enter the space between the volute tongue and the impeller. Once the distance between the tongue and the impeller is large enough, the flow is trapped in the space between the impeller and the volute resulting in higher losses. If the distance became too small, strong pressure oscillations might occur in the blade pass frequency in vicinity of the tongue. Usually, the base circle diameter is expressed using D_3/ D_2 ratio. For special pumps like centrifugal pumps, based on the guidelines provided by Stepanoff [27], the proposed ratio is equal to 1.05. The value for the studied standard pump model is equal to 1.067. Another method to express the diameter of the volute base circle through the definition of radial gap δ, is provided below [10]:

$$\delta = \frac{D_3 - D_2}{D_2} \times 100\% \tag{15}$$

This parameter can reflect the radial clearance between the impeller and the tongue, clearly. Another important parameter is the volute tongue region. This value for the standard pump models is 6.67%. The local effect of the tongue on the volute flow pattern can be provided by the tongue shape and the peripheral angular position known as the volute advance angle.

The tip of the volute tongue is defined by a semicircle, and the tongue thickness is the diameter of this semicircle arc. According to Wesche [28], the effect of the tongue on the flow is heavily depended on the tongue thickness. The parametric studies have been conducted by displacement of the tongue angular position along the original profile curve in two positions with 22.5 ^{o} angle difference compared to the standard mode, including three general positions as shown in Table (6). By increasing the tongue angle, an attempt has been made to keep the radial gap between the impeller and the tongue at 6.67% but due to the flow line curve in the volute at the angular position of 80 °, the radial gap is increased by 9.09% However, when the throttle surface is adjusted from B_1 tongue to C_1 tongue, the area ratio is reduced from 5.83 to 2.77. The previous parametric studies using different tongue profiles have been carried out by substituting the 3mm and the 6mm leading edge thicknesses and the previous same conditions. The summary of the tongue profiles using the three mentioned positions have been provided as shown in Tables (7, 8). Changes in the pump performance curves have been shown in Figures (9, 10) with multiple tongue profiles in various flow rates and angular positions. For better perception of head variations and efficiency changes per flow rate, tongues with the same thickness and various angular positions have been provided in separate diagrams. It can be seen clearly that changes in tongue profiles from tongue A to C could result in flow rate augmentation.

Table 6 Angular features of three types of tongue in 1mm leading edge thickness

Tongue type	Tongue-B_1	Tongue-A_1	Tongue-C_1
Radial gap $\delta(\%)$	6.67	6.67	10.30
Tongue edge diameter $D_T(mm)$	1	1	1
Tongue advance angle $\varphi_T(deg)$	40	62.5	85
Impeller outlet area $F_2(mm^2)$	3460.22	3460.22	3460.22
Throttle area $F_T(mm^2)$	593.45	583.22	1250.68
Area ratio $Y = F_2/F_T$	5.83	5.93	2.77

Table 7 Angular features of three types of tongue in 3mm leading edge thickness

Tongue type	Tongue-B_3	Tongue-A_3	Tongue-C_3
Radial gap $\delta(\%)$	6.67	6.91	10.30
Tongue edge diameter $D_T(mm)$	3	3	3
Tongue advance angle $\varphi_T(deg)$	40	62.5	85
Impeller outlet area $F_2(mm^2)$	3460.22	3460.22	3460.22
Throttle area $F_T(mm^2)$	551.28	651.58	1308.11
Area ratio $Y = F_2/F_T$	6.28	5.31	2.65

Table 8 Angular features of three types of tongue in 6mm leading edge thickness

Tongue type	Tongue-B_6	Tongue-A_6	Tongue-C_6
Radial gap $\delta(\%)$	6.67	7.03	10.54
Tongue edge diameter $D_T(mm)$	6	6	6
Tongue advance angle $\varphi_T(deg)$	40	62.5	85
Impeller outlet area $F_2(mm^2)$	3460.22	3460.22	3460.22
Throttle area $F_T(mm^2)$	488.67	651.58	1269.68
Area ratio $Y = F_2/F_T$	7.08	5.31	2.73

Meanwhile, when tongue A is replaced with tongue B, the head is clearly reduced. In higher flow rate conditions, an increase in the flow rate could lead to an obvious head loss, resulting in more linear curves. However, when tongue A is substituted for tongue C, the head increase become less. Once tongue B is substituted for tongue C, the hydraulic efficiency is slowly improved as shown in Figure (10), and also the high efficiency range is increased. In addition, conditions of optimal efficiency are shifted along the higher flow rates, however, the extent of efficiency change when the tongue is shifted from B to A is much larger than A to C.

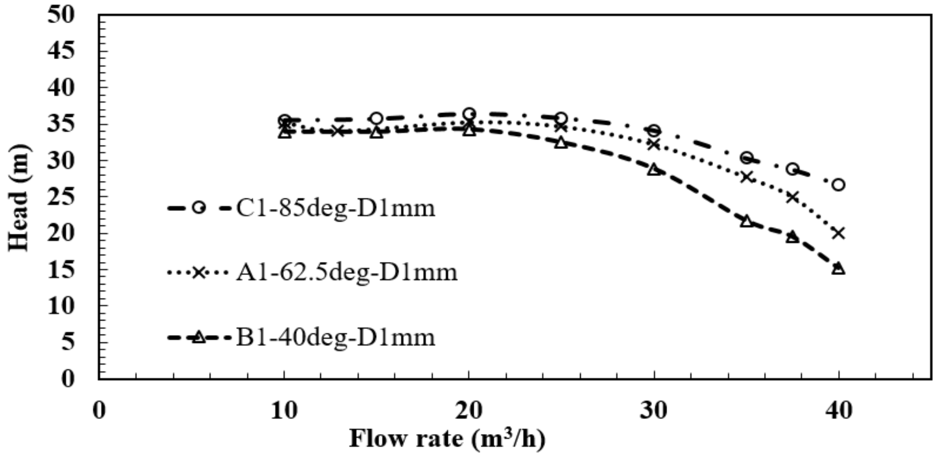

a

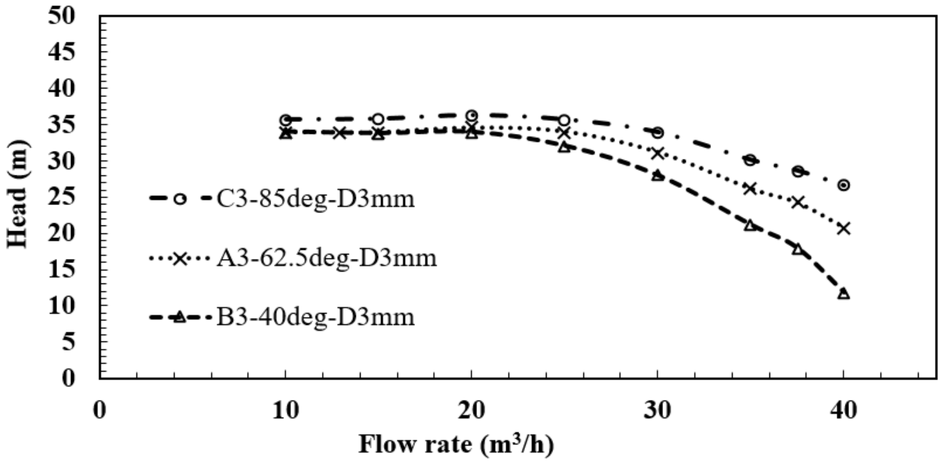

b

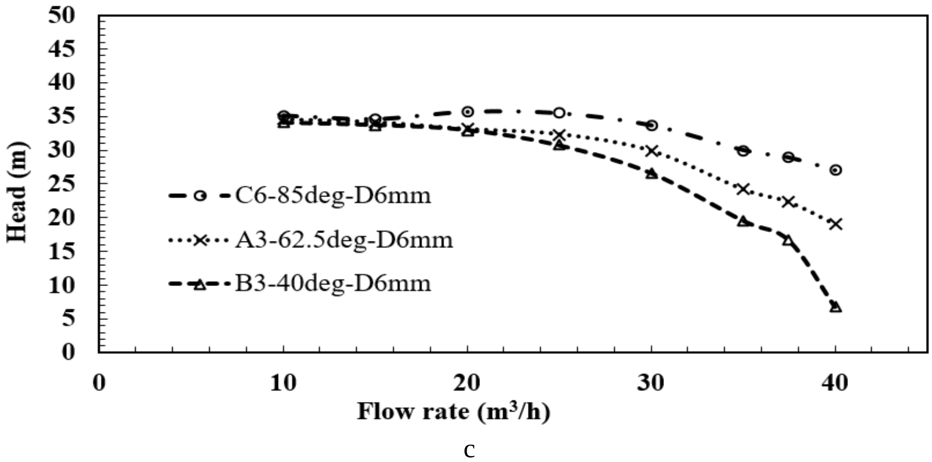

c

Figure 9 Hydraulic performance curves of pump head per various flow rates in multiple angular positions with tongue thicknesses of a) 1mm, b) 3mm and c) 6mm.

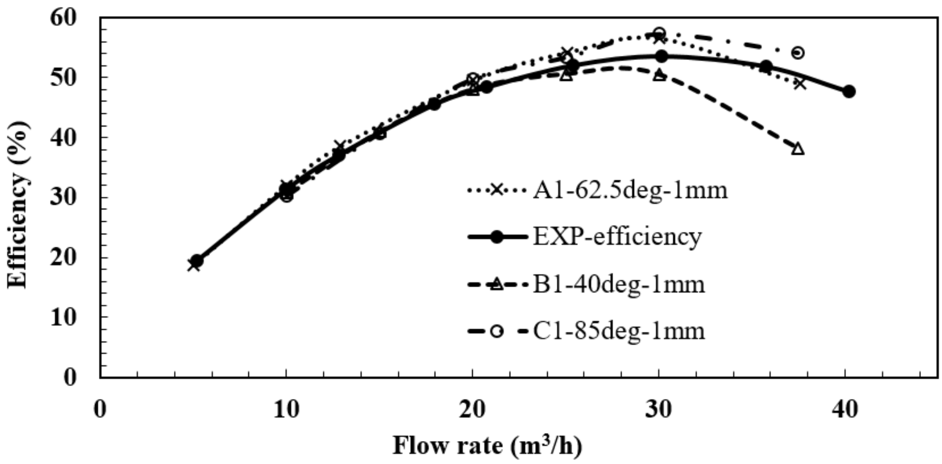

Figure 10 Hydraulic performance curves of pump efficiency per various flow rates in multiple angular positions with tongue thickness of 1mm.

For better understanding of head and efficiency variations per flow rate, tongues with the same angular position but various thicknesses have been provided on Figures (11,12), respectively. It can be seen that, by changing the tongue thickness from 1 mm to 6 mm, in angular positions of 40 ° and 62.5 °, the head is also reduced at the same flow rate as the same occurrence happening to efficiency diagram in 62.5 ° tongue angle. Meanwhile, in the angular position of 85 °, when tongue diameter of 1 mm is substituted for a 6 mm one, the head variations are not obvious. In higher flow rate conditions, an increase in the flow rate results in an obvious head loss and also a more linear head curve. Also, the thickness variations in 85 ° have the lowest impact on the overall pump performance and optimum efficiency conditions are transferred toward the higher flow rates.

Figure (13) shows a two-dimensional view of the velocity vector in the volute casing near the tongue region for various flow rates. It is quite obvious that in the design flow rates, the velocity vectors around the blade have the same value and direction, and compatibility and adjustment between the direction of the diffuser inflow and the volute tongue angle is very appropriate. From the stagnation point at the tip of the tongue, the fluid is slowly entered the diffuser and also diffused in the radial gap between the impeller and the volute tongue along the tangential path. In addition, there is also no signs of flow separation or vortex in vicinity of the tongue, but what is shown in Figure (13) in the off-design conditions, the inflow path to the diffuser is not compatible with the tongue angle, and the incidence angle is revealed. In lower flow rates, a part of fluid is rotated at the diffuser in vicinity of the volute tongue into the volute casing toward the radial gap, and a stagnation point in the tongue advance edge is formed in vicinity of the diffuser. Besides, it will also establish an unstable cavitation. However, in higher flow rates, most of the fluid in vicinity of the tongue flows within the diffuser toward the outflow of impeller, and the stagnation point is on the tongue advance leading edge near the volute casing. The result which is also compatible with various tongue angles would verify that the location change of the stagnation point around the tip of the tongue is only depended on the change in the flow rate conditions and is free of tongue profile variation. However, it could be revealed that by reducing the tongue angle, the location of the vortex and backflow in the higher flow rates goes further away from the tongue.

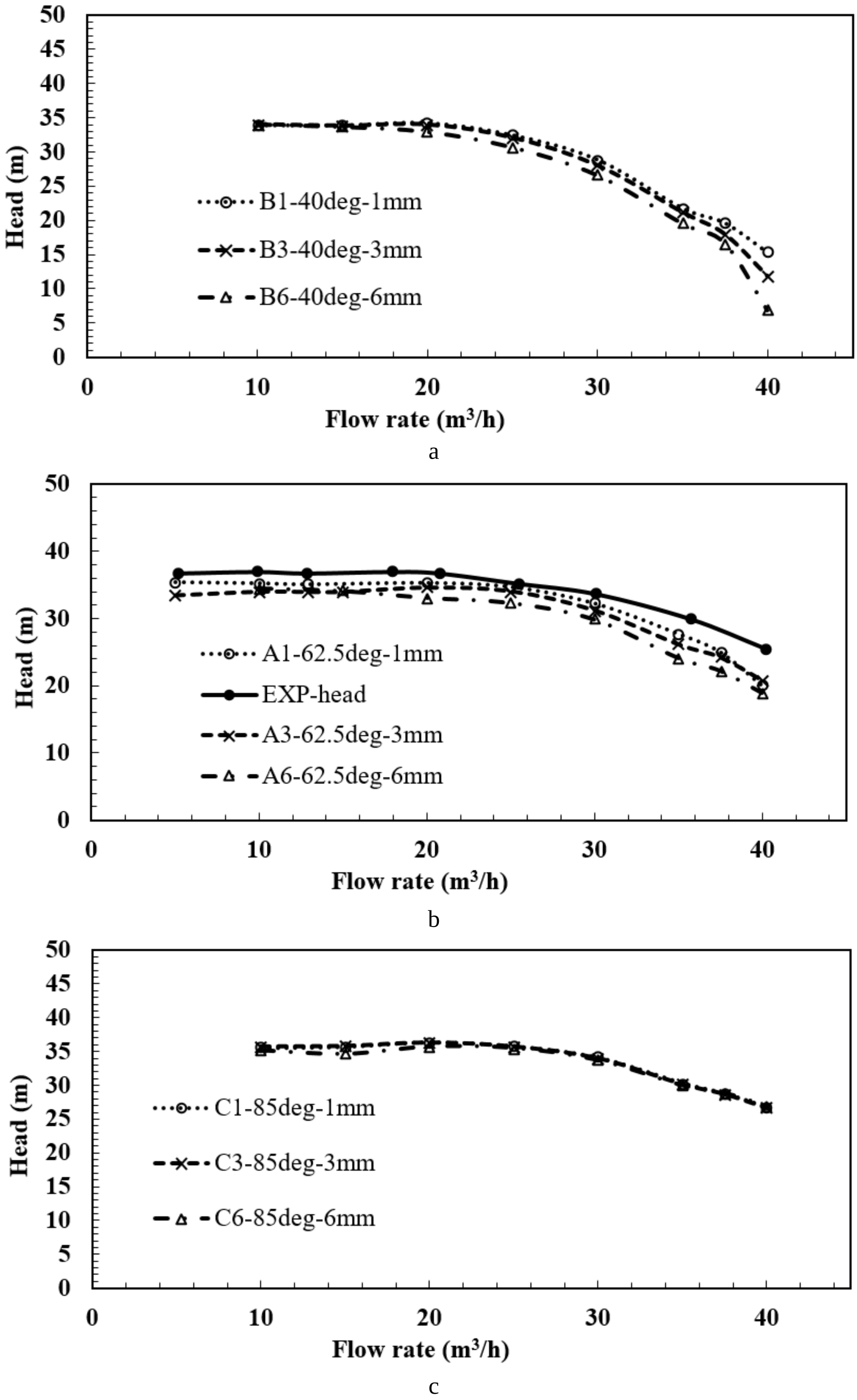

Figure 11 Hydraulic performance curves of pump head per various flow rates in multiple tongue thicknesses with angular positions of a) 40 °, b) 62.5 °, c) 85 °.

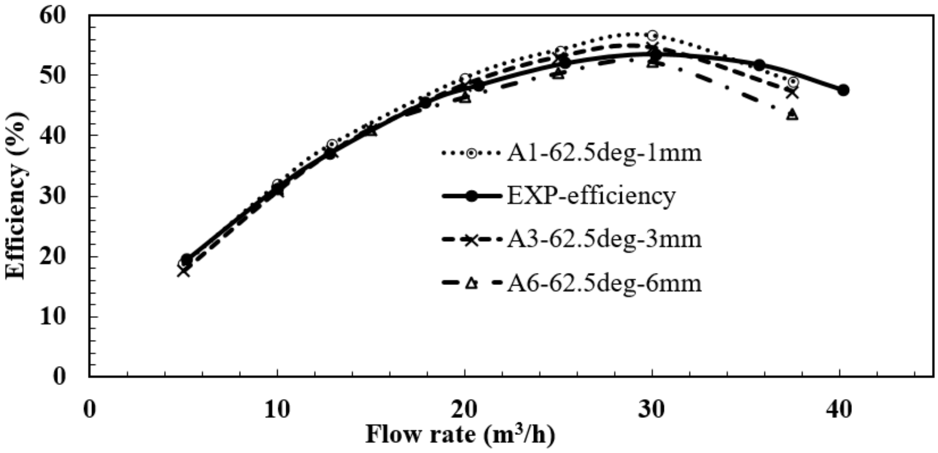

Figure 12 Hydraulic performance curves of pump efficiency per various flow rates in multiple tongue thicknesses with angular position of 62.5 °.

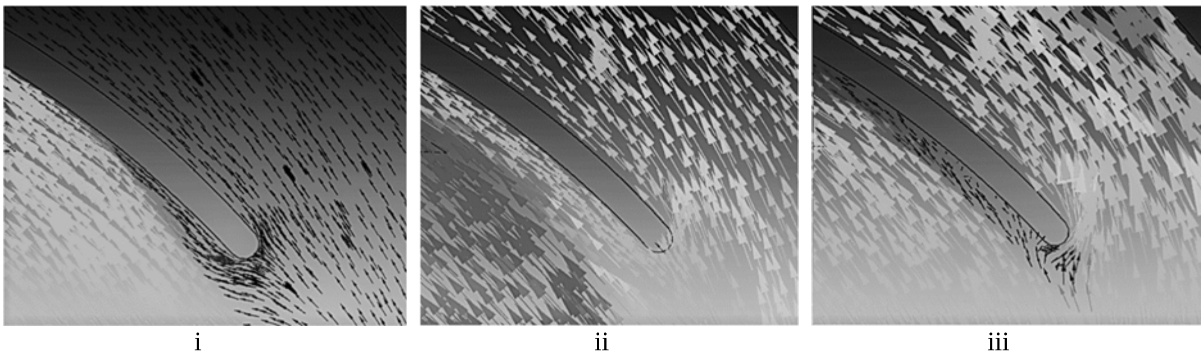

Figure 13 Velocity distribution in near the tongue region for angular position of 40 ° and diameter of 3mm in i) 0.4Q_d ii) Q_d iii) 1.4Q_d flow rate.

For the low flow rate, 40% of the value Q_d, the velocity vectors in vicinity of the tongue pass the tongue and moves toward the blade. This phenomenon is due to the pressure increase around the blades from tongue toward the outlet. Thus, the stagnation point in vicinity of the tongue will be located toward the throttle. In the high flow rate, 140% of the value Q_d, a circulation area can be seen in the downstream of the volute throttle from the volute tongue showing the separation of the boundary layer. So, most of the velocity vectors at the tongue pass through the discharge area. This phenomenon approves the boundary layer separation in the near-tongue region for high flow rates. The absolute velocity direction in the blade trailing edge, facing the tongue shape, is diverted from the zero angle which results in an incidence angle that is raised by increasing the flow rate. Since the flow angle is so much larger than the tongue zero incidence angle, the stagnation point is shifted from the leading edge of the tongue to another position on the tongue side toward the impeller (internal section). The low-pressure area progresses on the other side toward the volute discharge and the cavitation formation. As shown in Figure (14), the vapor structure in the impeller cross section in the interface of the pump model in vicinity of the tongue at the flow rate of 140% of the design value (Q_d) are quite obvious despite the overall input pressure of 101325 Pa in the angular position of 40° and various thicknesses. In such operating point, there is no cavitation in the pump impeller, so the total head loss of 3% is the result of cavitation in the volute tongue.

According to Figure (15), in low angular position of tongue, 40 °, and tongue thickness of 3 mm, the results show that a cloud cavitation as seen in individual hydrofoils [29] is revealed on the tongue. An alternative evolution process of the cavitation structures, from the elementary to advanced stage, could be found with cloud cavitation shedding along each blade passage in Bachert et al. [13] research. The results indicate that a greater focus on possible emergence of cavitation on the volute tongue in off-design conditions and low angular positions is required since the cavitation position can merely cause 3% head loss. Additionally, the appearance of unstable cavitation in the higher pressure loss areas such as the pump volute, can cause an erosion and a severe corrosion to the solid surfaces.

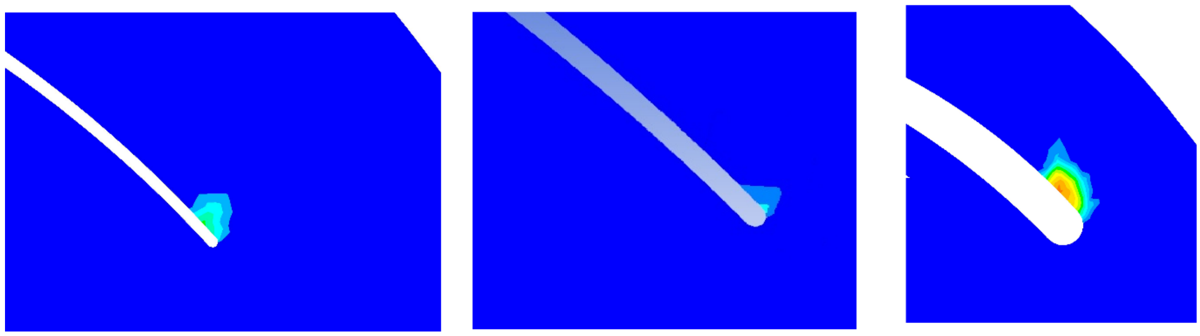

a b c

Figure 14 Vapor structure in the impeller cross section on the interface of the pump model in vicinity of the tongue at the flow rate of 140% of the design value (Q_d) with overall input pressure of 101325 Pa in the angular position of 40° with tongue thickness of a) 1 mm (B_1), b) 3mm (B_3), c) 6 mm (B_6).

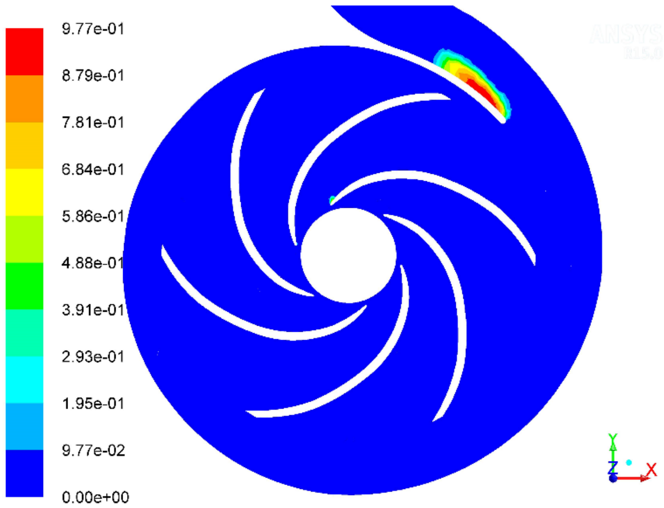

Figure 15 Vapor structure in vicinity of the tongue in the angular position of 40° and tongue thickness of 3 mm at overall input pressure of 101325 Pa and the flow rate of 160% of the design value (Q_d).

In the above-mentioned cavitation analysis in the design condition and different angular positions of the tongue in the testing pump, three causes that have not been studied widely so far are responsible for this phenomenon. According to this research, these causes which have been identified by studying various flow features are as follows:

1) Increased pressure due to the impeller is heavily decreased by increasing the design flow rate. This means that the static pressure in vicinity of the tongue in overload conditions become lower and that make the system prone to cavitation.

2) In the flow rates higher than the optimum rate, the absolute velocity direction in the trailing edge of blade is diverted from the zero angle against the tongue shape. It leads to a greater impact angle increasing by the raised flow rate. Since the flow angle is so much larger than the zero impact angle of the tongue, the stagnation point is shifted from the tongue leading edge to another position on the side of the tongue toward the impeller (internal part). The low-pressure area progresses on the front side toward the volute discharge and formation of cavitation.

3) In addition, the blade passage of the impeller causes an alternative velocity field and a variable pressure in vicinity of the tongue. The unstable flow field is prone to cavitation with a different impact on the various cavitation phenomena in the tongue. For instance, the unstable cavitation is known as the most erosive cavitation [30], so it is not surprising that sometimes local erosion damage at the centrifugal pumps tongue can be found after working in an overload condition for prolonged time frequencies [31].

5 Conclusion

In this research, the hydraulic performance of centrifugal pumps for various tongue profiles were numerically investigated using ANSYS-Fluent software in off-design conditions. The $k-\omega$ turbulence model with a hybrid grid, which agreed well with the experimental results, was chosen for analysis of a steady flow through a centrifugal pump model. Various tongue angles and thicknesses were examined to study the influence of tongue geometrical parameters on the head, efficiency, velocity distribution and cavitation structure in various flow rates. Results showed that, volutes with higher tongue angles have higher pump head and better efficiency at the same flow rate, i.e., changing the tongue angle from 40° to 85° with 1mm tongue thickness on 35 m^3/h flow rate would result in about 15% and 10% increase in the pump efficiency and head, respectively. Also, reducing the tongue thickness did not result in a significant change in head or efficiency but improved them in total, e.g., substituting the 6mm tongue thickness for a 1mm one in 62.5° tongue angle on 35 m^3/h flow rate would hardly increase both the efficiency and the head by 5%. Nevertheless, the head and efficiency of the pump in different tongue profiles have the most variations in higher flow rate ranges. Furthermore, the velocity distributions near the tongue region indicated that the inflow path to the diffuser is not compatible with the tongue angle, in off-design conditions resulting in vortices and backflows appearance.

Also, the cloud cavitation simulation confirmed that there are no signs of cavitation in the impeller in higher flow rates, lower tongue angles and various tongue thicknesses, and the volute tongue cavitation is the cause of the 3% head loss.

Declaration of conflicting interests

The author(s) declared no potential conflicts of interest with respect to the research, authorship, and/or publication of this article.

Funding

This research received no specific grant from any funding agency in the public, commercial, or non-for-profit sectors.

References

[1] Neumaier, R., "*Hermetic Pumps, the* Latest *Innovations and Industrial Applications of Sealless Pumps*", Houston, TX: Gulf Publishing Company, (1997).

[2] Gülich, J.F., "*Centrifugal Pumps*", Springer, (2008).

[3] Gonzalez, J., Fernández, J., Blanco, E., and Santolaria, C., "Numerical Simulation of the Dynamic Effects Due to Impeller-volute Interaction in a Centrifugal Pump", Journal of Fluids Engineering, Vol. 124, pp. 348-355, (2002).

[4] Lorett, J., and Gopalakrishnan, S., "Interaction between Impeller and Volute of Pumps at Off-design Conditions", Journal of Fluids Engineering, Vol. 108, pp. 12-18, (1986).

[5] Blake, J.R., and Gibson, D., "Cavitation Bubbles near Boundaries", Annual Review of Fluid Mechanics", Vol. 19, pp. 99-123, (1987).

[6] Fu,Y., Yuan, J., Yuan, S., Pace, G., d'Agostino, L., Huang, P., and Li, X., "Numerical and Experimental Analysis of Flow Phenomena in a Centrifugal Pump Operating under Low Flow Rates", Journal of Fluids Engineering, Vol. 137, pp. 011102, (2015).

[7] Grist, E., "*Cavitation and the Centrifugal Pump: A Guide for Pump users*", CRC Press, Taylor and Francis, USA, (1998).

[8] Hira, D. S., and Vasandani, V. P., "Influence of Volute Tongue Length and Angle on the Pump Performance", Journal of the Institution of Engineers (India), Part M.E. No. 56, pp. 55-59, (1975).

[9] Gonzáles, J., Santolaria, C., Parrondo, J.L., Fernández, J., and Blanco, E., "Unsteady Radial Forces on the Impeller of a Centrifugal Pump with Radial Gap Variation", ASME/JSME 2003 4th Joint Fluids Summer Engineering Conference, American Society of Mechanical Engineers, pp. 1173-1181, Honolulu, Hawaii, USA, (2003).

[10] Wong, Y.W., Chan, W.K., and Hu, W.J., "Effects of Tongue Position and Base Circle Diameter on the Performance of a Centrifugal Blood Pump", Artificial Organs, Vol. 31, pp. 639-645, (2007).

[11] Guo, P., Luo, X., Liao, W., and Zhu, G., "Numerical Investigation on Impeller-volute Interaction in the Centrifugal Pump with Radial Gap and Tongue Profile Variation", ASME 2008 Fluids Engineering Division Summer Meeting Collocated with the Heat Transfer, Energy Sustainability, and 3rd Energy Nanotechnology Conferences, American Society of Mechanical Engineers, pp. 217-224, Jacksonville, Florida, USA, (2008).

[12] Barrio, R., Parrondo, J., Blanco, and Blanco, E., "Numerical Analysis of the Unsteady Flow in the Near-tongue Region in a Volute-type Centrifugal Pump for Different Operating Points", Computer and Fluid, Vol. 39, pp. 859-870, (2010).

[13] Bachert, R., Stoffel, B., and Dular, M., "Unsteady Cavitation at the Tongue of the Volute of a Centrifugal Pump", J. Fluid Eng., Vol. 132, pp. 061301-061306, (2010).

[14] Alemi, H., Nourbakhsh, S.A., Raisee, M., Dehkordi, M.S., and Najafi, A., "Effect of the Volute Tongue Profile on the Performance of a Low Specific Speed Centrifugal Pump", Proceedings of the Institution of Mechanical Engineers Part A: Journal of Power and Energy, Vol. 229, pp. 210-220, (2015).

[15] Gu, Y., Yuan, S., Pei, J., Zhang, J., and Zhang, F., " Effects of the Impeller–volute Tongue Interaction on the Internal Flow in a Low-specific-speed Centrifugal Pump with Splitter Blades", Proceedings of the Institution of Mechanical Engineers Part A: Journal of Power, and Energy, Vol. 232, pp. 170-180, (2018).

[16] Jia, X., Cui, B., Zhu, Z., and Yu, X., "Numerical Investigation of Pressure Distribution in a Low Specific Speed Centrifugal Pump", Journal of Thermal Science, Vol. 27, pp. 25-33, (2018).

[17] Yan, S., Luo, X., Zhang, L., and Li, C., "Numerical Analysis of the Double Suction Centrifugal Pump with Different Tongue Shape", IOP Conference Series: Earth and Environmental Science, IOP Publishing, Beijing, China, (2018).

[18] Oro, J.F., González, J., Perotti, R.B., and Vega, M.G., "Numerical Analysis of the Deterministic Stresses Associated to Impeller-tongue Interactions in a Single Volute Centrifugal Pump", Journal of Fluids Engineering, Vol. 141, pp. 091104-091116, (2019).

[19] Arani, H.A., Fathi, M., Raisee, M., and Nourbakhsh, S.A., "Numerical Investigation of Tongue Effects on Pump Performance in Direct and Reverse Modes", IOP Conference Series: Earth and Environmental Science, IOP Publishing, (2019).

[20] Zwart, P.J., Gerber, A.G., and Belamri,T., "A Two-phase Flow Model for Predicting Cavitation Dynamics", Fifth International Conference on Multiphase Flow, Yokohama, Japan, (2004).

[21] Wan, B., Benra, F.K., and Dohmen, H.J., "Application of a New Numerical Solver to Turbomachinery Flow Problems", Proceedings of the Institution of Mechanical Engineers, Part A: Journal of Power and Energy, Vol. 227, pp. 628-636, (2013).

[22] Kozubková, M., Rautová, J., and Bojko, M., "Mathematical Model of Cavitation and Modelling of Fluid Flow in Cone", Procedia Engineering, Vol. 39, pp. 9-18, (2012).

[23] Gerber, A., "A CFD Model for Devices Operating under Extensive Cavitation Conditions", ASME International Mechanical Engineering Congress and Exposition, American Society of Mechanical Engineers, pp. 341-349, New Orleans, LA, 17-22 November, (2002).

[24] Friedrichs, J., and Kosyna, G., "Rotating Cavitation in a Centrifugal Pump Impeller of Low Specific Speed", J. Fluid Eng., Vol. 124, pp. 356-362, (2002).

[25] Friedrichs, J., and Kosyna, G., "Unsteady PIV Flow Field Analysis of a Centrifugal Pump Impeller under Rotating Cavitation", Fifth International Symposium on Cavitation (Cav 2003) Osaka, Japan, November, (2003).

[26] Hofmann, M., Stoffel, B., Friedrichs, J., and Kosyna, G., "Similarities and Geometrical Effects on Rotating Cavitation in Two Scalted Centrifugal Pumps", Fourth International Symposium on Cavitation, California Institute of Technology, June 20-23, (2001).

[27] Stepanoff, A.J., "*Centrifugal and Axial Flow Pumps: Theory, Design, and Application*", Wiley, New York, (1957).

[28] Wesche, W., "Measurements on a Helical Casing of a Centrifugal Pump", World Pumps, pp. 321-324, (1987).

[29] Kubota, A., Kato, H., and Yamaguchi, M., "A New Modelling of Cavitating Flows: a Numerical Study of Unsteady Cavitation on a Hydrofoil Section", J. of Fluid Mechanic, Vol. 240, pp. 59-96, (1992).

[30] Dular, M., Bachert, B., Stoffel, B., and Širok, B.J.W., "Relationship between Cavitation Structures and Cavitation Damage", Wear, Vol. 257, pp. 1176-1184, (2004).

[31] Brennen, C.E., "*Hydrodynamic of Pump*", Oxford University Press, (1994).